PERIÓDICO TCHÊ QUÍMICA

ARTIGO ORIGINAL

SÍNTESE DE NOVOS ADSORVENTES VIA MCM-41 FUNCIONALIZADO PARA A REMOÇÃO DE ALGUNS ÍONS DE SOLUÇÕES AQUOSAS

SYNTHESIS OF NEW ADSORBENTS VIA FUNCTIONALIZED MCM-41 FOR THE REMOVAL OF SOME IONS FROM AQUEOUS SOLUTION

تحضير مواد مازة جديدة بواسطة توظيف MCM-41 لازالة بعض الايونات من المحاليل المائية

Raghad Saad Hatem*
Department of Chemistry, College of Science, University of Kerbala, Kerbala, Iraq.

Alaa Frak Hussain
Department of Chemistry, College of Science, University of Kerbala, Kerbala, Iraq.

Hayder Hamied Mihsen
Department of Chemistry, College of Science, University of Kerbala, Kerbala, Iraq.

** Corresponding author*
Raghad.saad@uokerbala.edu.iq

Received on February 28, 2024; received as revised form 07 April; 02 May; accepted June 12, 2024.

RESUMO

Introdução: Materiais mesoporosos como a sílica MCM-41 são muito apreciados por suas características estruturais e aplicações em adsorção e catálise. Este estudo melhora a capacidade da MCM-41 de adsorver íons de cobalto e cobre, introduzindo grupos amina e base de Schiff, aumentando sua afinidade por esses poluentes e auxiliando na sua remoção de soluções aquosas. **Objetivos**: Preparar MCM-41@NTPE e MCM-41@NTPE-BSAL e utilizá-los para adsorver poluentes pesados como íons divalentes de cobalto e cobre de soluções aquosas. **Métodos**: Materiais mesoporosos (MCM-41@NTPE e MCM-41@NTPE-BSAL) derivados de cinzas de casca de arroz foram utilizados como adsorventes de baixo custo para a adsorção de íons Co(II) e Cu(II) de soluções aquosas. Experimentos de adsorção foram realizados para determinar parâmetros como concentração de íons, pH, tempo de exposição e massa de adsorvente. **Resultados**: MCM-41@NTPE e MCM-41@NTPE-BSAL foram caracterizados por FT-IR, FESEM-EDX, TEM, adsorção-dessorção de N2, DRX e TGA/DTA. O FT-IR confirmou a presença de grupos silanol e siloxano. DRX e TEM indicaram arranjos hexagonais altamente ordenados. A análise de adsorção-dessorção de N2 revelou diâmetros médios de poros de 42,468 nm e 40,417 nm, volumes totais de poros de 0,094 cm^3g^{-1} e 0,3384 cm^3g^{-1}, e áreas superficiais específicas de 8,873 m^2g^{-1} e 37,802 m^2g^{-1} para MCM-41@NTPE e MCM-41@NTPE-BSAL, respectivamente. A TGA mostrou três etapas de redução de massa. A avaliação da adsorção mostrou que pH 6 e 5 foram ótimos para a adsorção de Co(II) e Cu(II), respectivamente, e a adsorção aumentou com a concentração inicial e o tempo de exposição. **Discussão**: A DRX confirmou a estrutura mesoporosa hexagonal, enquanto a análise BET exibiu naturezas amorfas. A TGA sugeriu que MCM-41@NTPE e MCM-41@NTPE-BSAL têm potencial de estabilidade, embora se decomponham entre 15-900°C. A microscopia eletrônica revelou arranjos hexagonais ordenados. Os materiais demonstraram alta eficácia na extração de íons de cobre e cobalto de soluções aquosas. **Conclusões**: Dois materiais de sílica mesoporosa (MCM-41@NTPE e MCM-41@NTPE-BSAL) foram preparados a partir de casca de arroz pela funcionalização da MCM-41. A avaliação da adsorção mostrou que a adsorção dependia do tempo de exposição, pH, concentração inicial e massa de adsorvente. MCM-41@NTPE-BSAL exibiu melhor adsorção de íons do que MCM-41@NTPE.

Palavras-chave*: Tratamento de águas residuais, materiais mesoporosos, MCM-41, área superficial, síntese de biomateriais.*

ABSTRACT

Background: Mesoporous materials like MCM-41 silica are highly regarded for their structural features and applications in adsorption and catalysis. This study enhances MCM-41's ability to adsorb cobalt and copper ions

DOI: 10.52571/PTQ.v21.n47.2024_04_HATEM_pg_42_60.pdf

by introducing amine and Schiff-base groups, boosting its affinity for these pollutants and aiding in their removal from water solutions. **Aims**: To prepare MCM-41@NTPE and MCM-41@NTPE-BSAL and use them to adsorb heavy pollutants like cobalt and copper divalent ions from aqueous solutions. **Methods**: Mesoporous materials (MCM-41@NTPE and MCM-41@NTPE-BSAL) derived from rice husk were used as low-cost adsorbents for the adsorption of Co(II) and Cu(II) ions from aqueous solutions. Uptake experiments were performed to determine adsorption parameters like ion concentration, pH, exposure time, and adsorbent mass. **Results**: MCM-41@NTPE and MCM-41@NTPE-BSAL were characterized by FT-IR, FESEM-EDX, TEM, N_2-adsorption–desorption, XRD,AFM and TGA/DTA. FT-IR confirmed the presence of silanol and siloxane groups. XRD and TEM indicated highly ordered hexagonal arrangements. N_2–adsorption–desorption analysis revealed average pore diameters of 42.468 nm and 40.417 nm, total pore volumes of 0.094 cm^3g^{-1} and 0.3384 cm^3g^{-1}, and specific surface areas of 8.873 m^2g^{-1} and 37.802 m^2g^{-1} for MCM-41@NTPE and MCM-41@NTPE-BSAL, respectively. TGA showed three mass reduction steps. Adsorption assessment showed pH 6 and 5 were optimal for Co(II) and Cu(II) uptake, respectively, and uptake increased with initial concentration and exposure time. **Discussion**: XRD confirmed the hexagonal mesoporous structure, while BET analysis displayed amorphous natures. TGA suggested MCM-41@NTPE and MCM-41@NTPE-BSAL have potential for stability, although decomposing between 15-900°C. Electron microscopy revealed ordered hexagonal arrangements. The materials demonstrated high efficacy in extracting copper and cobalt ions from aqueous solutions. **Conclusions**: Two mesoporous silica materials (MCM-41@NTPE and MCM-41@NTPE-BSAL) were prepared from rice husk by functionalizing MCM-41. Adsorption assessment showed uptake depended on exposure time, pH, initial concentration, and adsorbent mass. MCM-41@NTPE-BSAL exhibited better ion uptake than MCM-41@NTPE.

Keywords: *wastewater treatment, mesoporous materials, MCM-41, surface area, uptake*.

خلاصة

مقدمة :المواد المسامية مثل السيليكا MCM-41 تحظى بتقدير كبير بسبب خصائصها الهيكلية وتطبيقاتها في الامتزاز والتحفيز .تهدف هذه الدراسة إلى تحسين قدرة MCM-41 على امتصاص أيونات الكوبلت والنحاس من خلال إدخال مجموعات الأمين وقاعدة شيف، مما يزيد من جاذبيتها لهذه الملوثات ويساعد في إزالتها من المحاليل المائية .**الأهداف :**تحضير MCM-41@NTPE و MCM-41@NTPE-BSAL واستخدامهما لامتصاص الملوثات الثقيلة مثل أيونات الكوبلت والنحاس ثنائية التكافؤ من المحاليل المائية.**الطرق** :تم استخدام مواد مسامية MCM-41@NTPE و MCM-41@NTPE-BSAL مشتقة من قشور الأرز كممتصات منخفضة التكلفة لامتصاص أيونات الكوبلت والنحاس من المحاليل المائية .أجريت تجارب الامتزاز لتحديد معايير مثل تركيز الأيونات، ودرجة الحموضة، ووقت التعرض، وكتلة الممتز .**النتائج :**تم**تشخيص** MCM-41@NTPE و MCM-41@NTPE-BSAL بواسطةFT-IR ، وFESEM-EDX، وTEM، وN_2-adsorption–desorption وXRD، وAFM .وTGA/DTAأكد FT-IR وجود مجموعات السيلانول والسيلوكسان . أشارت XRD و TEMإلى ترتيبات سداسية عالية التنظيم .كشفت تحاليل امتزاز-إزالة النيتروجين عن أقطار متوسطة للمسام بحجم 42.468 نانومتر و 40.417 نانومتر، وحجم إجمالي للمسام قدره 0.094 سم³/جم و 0.3384سم³/جم، ومساحة سطحية محددة تبلغ 8.873 م²/جم و 37.802م²/جم لـ-MCM 41@NTPEو MCM-41@NTPE-BSALعلى التوالي .أظهر تحليل TGA ثلاث مراحل من تخفيض الكتلة .أظهرت تقييمات الامتزاز أن درجة الحموضة 6 و 5كانت مثالية لامتزاز أيونات الكوبلت والنحاس على التوالي، وأن الامتزاز ازداد مع زيادة التركيز الأولي ووقت التعرض.**المناقشة :**أكدت XRDعلى الهيكل السداسي المسامي، بينما أظهرت تحاليل BET طبيعة غير متبلورة .اقترحت TGA أن MCM-41@NTPE و-MCM-41@NTPE BSALلديهما استقرار محتمل، على الرغم من تحللهما بين 900-15 درجة مئوية .كشفت المجهر الإلكتروني عن ترتيبات سداسية منظمة .أظهرت المواد فعالية عالية في استخلاص أيونات النحاس والكوبالت من المحاليل المائية.**الاستنتاجات :**تم تحضير مادتين من السيليكا المسامية MCM-41@NTPE) و MCM-41@NTPE-BSALمن قشور الأرز من خلال تحويل .MCM-41 أظهرت تقييمات الامتزاز أن الامتزاز يعتمد على وقت التعرض، ودرجة الحموضة، والتركيز الأولي، وكتلة الممتز .أظهر MCM-41@NTPE-BSAL قدرة أفضل على امتزاز الأيونات مقارنة بـ.MCM-41@NTPE

كلمات مفتاحية : معالجة مياه الصرف الصحي, المركبات المسامية, MCM-41, مساحة السطح, سعة الاخذ

1. INTRODUCTION:

Progression in materials science has focused on synthesizing new adsorbents that can potentially be effective in water treatment. Combining two or more substances into a larger one in materials science has been demonstrated to be an exceeding effective approach to producing new materials with new effective properties. Mesoporous silica like SBA-15, HMS, MCM-41, and MCM-48 are considered excellent materials for these types of uses due to their large surface areas, limited pore size, and controlled pore dimension (Costa *et al*., 2020) In addition, desirable material properties can be achieved or enhanced by attaching appropriate functional groups to their surfaces. Various approaches have been applied to enhance mesoporous silica materials. Hybrid materials produced by combining organic and inorganic components have proven effective in obtaining valuable materials (Martínez-Carmona *et al*., 2020; Verma *et al*., 2020).

Considerable research has been undertaken on the performance of mesoporous materials concerning improving their application via functionalization with various groups.

Modifying the outer layers of mesoporous materials is very interesting because it can make the surface basic or acidic (Barczak *et al*., 2020; Nie *et al*., 2020). Two main methods are used to alter mesoporous materials: the direct method (also called the co-condensation method) and the post-synthesis method (also known as the grafting method) (Wang *et al*., 2008). Functionalization procedures during synthesis involve incorporating a coating agent onto the surface groups of porous materials, producing a liquid medium free of water (Luan *et al*., 2005). Various agents can be used to modify such surfaces, such as disilazanes (Yu & Zhai, 2009), trialkoxysilanes (Luan *et al*., 2005) and chlorosilanes (Mirji *et al*., 2006). The grafting method reduces the number and size of pores, where only a small number of functional groups can actually be attached (Chong *et al*., 2004). The final material gain is a more ordered pore structure than the co-condensation method (Bernardoni & Fadeev, 2011). The post-synthesis method involves the use of trialkoxysilanes with reactive functional groups such as aminopropyl and chloropropyl, which can be further modified on the surface via the attachment of porphyrins (Mureseanu *et al*., 2008), thio(Pérez-Quintanilla *et al*., 2006), heterocyclic species (Li *et al*., 2007), aldehydes(Mureseanu *et al*., 2008), and polyethylenimine (Kim *et al*., 2005). It is important to note that metal ions can be introduced into the mesoporous sieves using direct and post-synthesis methods (Dragoi *et al*., 2009).

In this work, mesoporous materials (MCM-41@NTPA and MCM-41@NTPA-BSAL) derived from rice husk ash, as low-cost adsorbents, were prepared and applied in the adsorption of cobalt(II) and cupper(II) metal ions from their aqueous solutions. Dosage mass of adsorbent, concentration, exposure time and pH were studied as a factors effect on the uptake of the ions

2. MATERIALS AND METHODS:

2.1. Materials and instrumental

2.1.1. Materials:

Rice husk (RH) was collected from nearby rice production manufacturers in AL-Najaf Governorate, Abbacy city. The substances used included cetyltrimethylammonium bromide (Merck, 95%), cobalt chloride hexahydrate (Merck, 98%), copper chloride dihydrate (Fluka, 99.8%), hydrochloric acid (Thomas Baker, Analar), toluene (Qrec, 99.5%), sodium hydroxide (Merck, 99%), ammonia (Qrec, 69%), acetic acid (BDH, 99.5%), nitric acid (BDH, 65%), absolute ethanol (Fluka, > 99%), acetone (Romal, 9.7%), *N*-[3-(trimethoxysilyl)propyl]ethylenediamine (Merck, 95%), and 5-bomosalicylaldehyde (Merck, 95%). All chemicals were of analytical grade and used without further purification.

2.1.2. Instrumental

Infrared spectroscopy (8400s Shimadzu "Japan, spectral range from 4000 to 400 cm^{-1}), N_2 adsorption-desorption analysis (Belsorp adsorption/desorption data analysis software BEL Japan, Inc.), powder X-ray diffraction ((Philips PW 1730/10) X-ray diffractometer using Cu Kα radiation), and scanning electron microscopy (SEM)-(FESEM MIRA III (TESCAN)/(Czech Republic)), transmission electron microscope (TEM)- EM 208S, PHILIPS, NEDERLAND, atomic force microscopy (AFM)- (NT-MDT/NTEGRA (Netherlands) and thermogravimetric analyses (TA instruments SDT-Q600 simultaneous TGA / DSC (België), from 30 to 900 °C at a heating rate of 20 °C min^{-1} under nitrogen flow. Also, the researchers used a UV-Vis Spectrometer (Shimadzu double beam 1800 UV) to determine (Co(II) and Cu(II) ions from its aqueous solutions

2.2. Methods

*2.2.*1 Preparation of sodium silicate and mesoporous silica (MCM-41) from rice husks.

First, the rice husk(RH) was washed with water to remove solid particles, mud and soil, then allowed to dry. A 30.0 gm of dried RH was added into a plastic container and treated with 500 mL, 1.0 M nitric acid for 24 h at room temperture. RH was then rinsed with distilled water to remove the acid until be neutral (pH=6-7) before drying in oven at 110 °C overnight. RH was stirred in 200 mL of 1.0 M NaOH for 24 h at room temperature. The mixture was filtered to obtain a dark filtrate (sodium silicate) which was kept in a covered plastic containerA sodium silicate solution was prepared from rice husks (Ali *et al*., 2023). A surfactant solution was produced by mixing 2.0 g of CTAB (cetyltrimethylammonium bromide) with 25 mL of deionized water. Silica surfactant solution was prepared by adding the filterate sodium silicate solution to surfactant solution under vigorous stirring at room temperature and adjusting the solution to pH 10 using CH_3COOH, then stirring at ambient temperature for 6 hours, followed by aging at a temperature of 100 °C for 24 hours. The final mixture was filtered use Buchner funnel and rinsed with deionized water before drying at 50 °C for 24 hours,than calcinated at 550 ± 3°C for 5 hours to eliminate the surfactant (Sutra & Brunel, 1996).

2.2.2 Synthesis of N-[3-(trimethoxysilyl) propyl] ethylenediamine functionalized mesoporous silica (MCM-41@NTPE)

1.0 g of MCM-41 was dried at 110°C in an oven for three hours to remove physisorbed moisture. 1.0 mL of *N*-[3-(trimethoxysilyl)propyl] ethylenediamine was added to the dried MCM-41 followed by addition of 30 mL toluene; this mixture was then refluxed for 24 hours at 110°C. The resulting solution contained a white solid filtered and washed with toluene, ethanol, and DMSO. Finally, the resultant powder was collected and labeled as MCM-41@NTPE.

2.2.3 Synthesis of 5-bromosalicylaldehyde-functionalized mesoporous silica (MCM-41@NTPE-BSAL)

To prepare MCM-41@NTPE-BSAL, a mixture of 2 g of 5-bromosalicylaldehyde and 1.0 g of MCM-41@NTPE was mixed with 30 mL of toluene. This mixture was refluxed at 110°C for 24 hours. The product was separated using a filter, rinsed with toluene followed by ethanol, and left to dry at 100°C for 24 hours. It was then crushed until it became a very fine powder labeled MCM-41@NTPE-BSAL. The steps to the overall preparation are shown in Scheme.

2.2.4. Analytical examinations

Fourier transform infrared technique (FTIR) was utilized to detect the functional groups within the structure of the compounds. Around one mg of the sample was grinded with KBr, then compress the sample with a piston. Wavelengths ranging from 400-4000 cm^{-1} were utilized.

XRD analysis was utilized to detect the crystalline structure of the compound. A 1.0 mg sample was made as a compact disk and inserted into the device for analysis.

SEM (scanning electron microscopy), AFM (Atomic force microscopy), TEM (transmission electron microscopy), and EDX (energy dispersive x-ray spectroscopy) analysis were applied to study the morphology, topography, particle shape, size, and composition of the compound.

The Brunauer-Emmett-Teller (BET) technique calculates the pore size and surface area. (BET) The method was used to calculate the surface area and pore size by passing nitrogen gas on 1 gm of compounds at an equal temperature after emptying the oven from pressure.

TGA (Thermogravimetric analysis) and DTA(differential thermal analysis) were utilized to determine the quantity of organically functionalized silica based on the weight change as a function of temperature.

2.2.5 Adsorption studies

MCM-41@NTPE and MCM-41@NTPE-BSAL, 0.1 g in each instance, were shaken with 50 mL of solutions of each metal ion, Co(II) and Cu(II). The amount of metal ions was determined by allowing the insoluble complex to settle and removing a specific amount of supernatant using a micropipette. The calibration curve for both ions was then constructed by preparing a series of dilutions for each ion to determine their uptake.

2.2.5.1 Effect of Exposure Time

The uptake capacity of 0.05 M Co(II) and 0.05 M Cu(II) solutions was determined by shaking 0.1 g each of MCM-41@NTPE and MCM-41@NTPE-BSAL with metal aqueous solutions for various times,

2.2.5.2 Effect of pH

Solutions of Co(II) (0.05 M) and Cu(II) (0.05 M) ions at various acidic functions, adjusted using NH_4OH (0.1 M)/HCL (0.1 M), were each shaken with 0.1 g of MCM-41@NTPE and MCM-41@NTPE-BSAL.

2.2.5.3 Effect of Concentration of Co(II) and Cu(II) Ions

Different concentrations of cobalt and copper ions were used to investigate the uptake capacity at different concentrations (0.02– 0.1 M) at optimized pH for both ions.

2.2.5.4 Effect of mass of the MCM-41@NTPE and MCM-41@NTPE-BSAL

The experiment was performed by taking different amounts of absorbent (0.1, 0.15, and 0.2 g per 50 mL) in the test solutions at optimized pH for both cobalt (0.05 M) and copper (0.05 M) ions.

3. RESULTS AND DISCUSSION:

3.1. Results

3.1.1. FTIR analysis

FT-IR spectra of MCM-41@NTPE and MCM-41@NTPE-BSAL are shown in Figure 1. Vibrations of the hydroxyl (-O-H) group of silanol (Si-OH) give rise to a characteristic band at approximately 3500 cm^{-1} (Si–OH).Trapped molecules of water give rise to a peak associated with a bending vibration at 1640 cm^{-1} (Adam & Batagarawa, 2013). The broad peak at 3000-3200 cm^{-1} corresponds to the free NH_2. The peaks at 3500 and 3450 cm^{-1} are attributed to the symmetric and asymmetric stretching vibrations of

the N-H bond of the primary amine. In contrast, the peaks at 3340 and 1655 cm^{-1} are attributed to the stretching and bending vibrations of the N-H bond in the secondary amine.

The FT-IR spectrum also exhibits bands at 445, 935, and 1090 cm^{-1}, characteristic of symmetric and anti-symmetric stretching of Si– O–Si (Carmona *et al*., 2013).

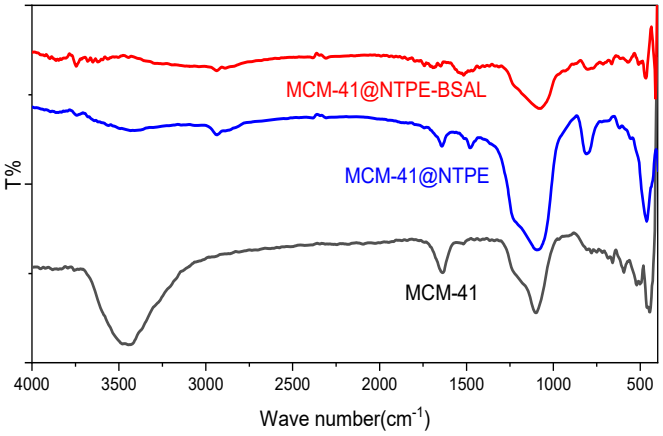

Figure 1. *FTIR spectra of MCM-41@NTPE and MCM-41@NTPE-BSAL.*

3.1.2. XRD analysis

The X-ray diffraction (XRD) analysis was carried out for the synthesized MCM-41@NTPE and MCM-41@NTPE-BSAL. The results of XRD analysis at low angle and high angle are presented in Figures 2 and 3, respectively.

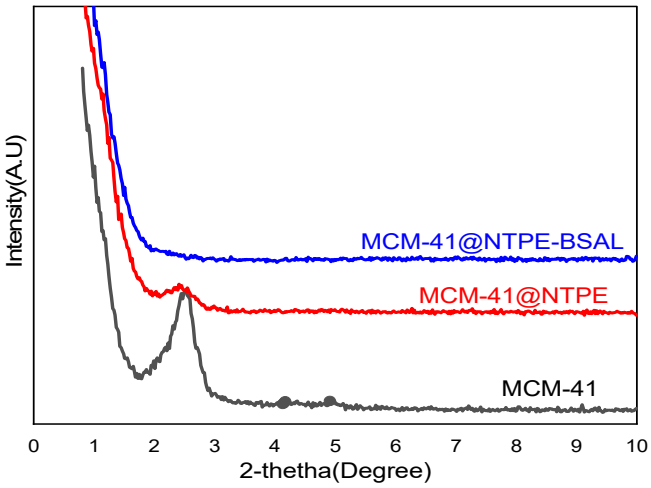

Figure 2. XRD spectra (low angle) of MCM-41, MCM-41@NTPE, and MCM-41@NTPE-BSAL.

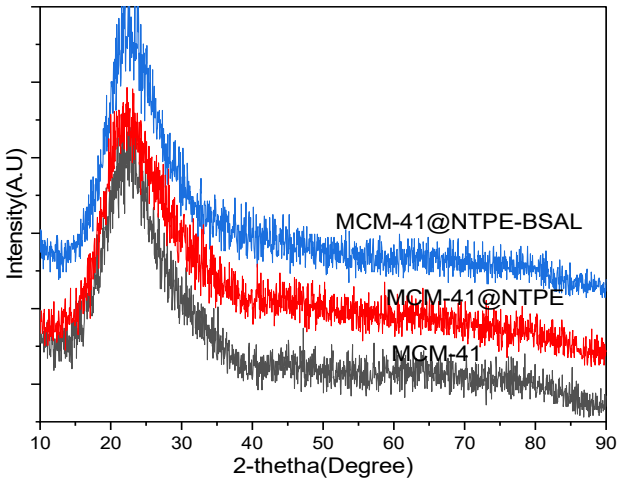

Figure 3. XRD spectra (high angle) of MCM-41, MCM-41@NTPE, and MCM-41@NTPE-BSAL

3.1.3. N2 Adsorption-Desorption Analysis

The surface area and the pore size distribution can be determined via N_2 adsorption–desorption analysis. From the results shown in Figures 4 and 5, the average pore diameters of MCM-41@NTPE and MCM-41@NTPE-BSAL are 42.468 nm and 40.417 nm, whilst the specific surface areas are 8.873 $m^2 \cdot g^{-1}$ and 37.802 $m^2 \cdot g^{-1}$, and the total pore volumes are 0.094 $cm^3 \cdot g^{-1}$ and 0.3384 $cm^3 \cdot g^{-1}$, respectively.

3.1.4. Analysis of SEM and EDX

SEM images of MCM-41@NTPE and MCM-41@NTPE-BSAL are shown in Figure 6.

Figure 7 also shows the EDX analysis of MCM-41@NTPE and MCM-41@NTPE-BSAL.

3.1.5. TEM Microscopy

TEM analysis was conducted to acquire further information regarding the structural characteristics of the MCM-41@NTPE and MCM-41@NTPE-BSAL (Figure 8).

3.1.6. AFM Analysis

The surface topographies of MCM-41@NTPE and MCM-41@NTPE-BSAL were demonstrated via the AFM analysis, as shown in Fig. 9.

3.1.7. Thermal Analysis

The thermal stabilities of MCM-41@NTPE and MCM-41@NTPE-BSAL were investigated via TGA analysis, as illustrated in Figure 10.

3.1.8. Adsorption studies

The effects of different variables on the metal ions, such as exposure time, pH, the concentration of metal ions, and the effect of the

mass of the MCM-41@NTPE and MCM-41@NTPE-BSAL, were investigated.

3.1.8.1 Effect of Exposure Time

The uptake capacity of Co(II) and Cu(II) solutions with MCM-41@NTPE and MCM-41@NTPE-BSAL are shown in Figure 11.

3.1.8.2 Effect of pH

It was observed that there was an increase in the uptake of metals with increasing pH. At pH 6, the highest uptake occurred for the Co(II) ion, while for Cu(II), this occurred at pH 5, as shown in Figures 12 and 13.

3.1.8.3 Effect of Concentration of Co(II) and Cu(II) Ions

Figures 14 and 15 illustrated the effect of different concentration of ions on the uptake of ions by MCM-41@NTPE and MCM-41@NTPE-BSAL.

3.1.8.4 Effect of mass of the MCM-41@NTPE and MCM-41@NTPE-BSAL

Figures 16 and 17 shows how the uptake of Co(II) and Cu(II) ions varied as adsorbent doses were increased from 0.1 to 0.2 g.

3.2. Disscusion

3.2.1. FTIR analysis

The spectra show the changes occurring in MCM-41 upon functionalization with N-[3-(trimethoxysilyl)propyl]ethylenediamine and, thereafter, with 5-bromosalicylaldehyde. The FT-IR spectrum of MCM-41, as shown in Figure 1, exhibits several bands typical of mesoporous silica. Figure 1 also shows the FTIR spectrum of MCM-41@NTPE-BSAL. The band associated with the O-H vibration is shifted to ~3400 cm^{-1}. The C-H aliphatic and aromatic group stretching vibrations were responsible for the clusters of low-intensity bands at ~3000 and 2500 cm^{-1} (Adam & Batagarawa, 2013). It was observed that the asymmetric vibration of the siloxane group gives a broad peak at 1107 cm^{-1}, while the silanol group gives rise to an asymmetric stretching peak at 965 cm^{-1} (Adam *et al*., 2010a). Additionally, stretches and bends of the siloxane group give rise to distinct peaks at 806 and 516 cm^{-1}(Adam & Iqbal, 2010). Three characteristic peaks at ~1000, ~800, and ~500 cm^{-1} are present in all spectra, which can also be attributed to the siloxane group (Attol *et al*., 2023). The FT-IR spectrum of MCM-41@NTPE showed that the number of absorption bands associated with silanol groups (Si-OH) at ~960 cm^{-1} were greatly reduced in intensity compared with those for MCM-41. This indicates successful anchoring of *N*-[3-(trimethoxysilyl)propyl]ethylenediamine (Adam *et al*., 2010). The presence of the azomethine C=N group was confirmed by a peak at 1640 cm^{-1}, indicating successful Schiff base ligand formation (Pervaiz *et al*., 2019). The peaks at 3523 and 3446 cm^{-1} were attributed to the symmetric and asymmetric stretching of the N-H bond of the primary amine, while the peaks at 3340 and 1655 cm^{-1} were attributed to the stretching and bending of N-H bond in the secondary amine of the same moiety.. The bands due to C–O vibrations usually appear in the vicinity of 1000–1300 cm^{-1}((Abbas *et al*., 2020a). However, after functionalization with 5-bromosalicylaldehyde, these bands overlapped with those of the siloxane group (Si–O–Si), although relatively small bands still appeared, as exhibited from the FT-IR spectrum of MCM-41. The N-H bending vibration (primary amine) appears at 1520 cm^{-1}, while the strong peak at 1380 cm^{-1} signifies the combination of stretches for the C-N group in primary amides. These bands show that there are propyl and amino groups on the silica (Sutra & Brunel, 1996).

3.2.2. XRD Analysis

The peak at approximately 2.17° (100) is attributed to a hexagonal mesoporous structure, characteristic of both MCM-41@NTPE and MCM-41@NTPE-BSAL (Figure 2). This can be seen in the TEM images shown in Figure 8. The intensity of the peaks recorded for MCM-41@NTPE and MCM-41@NTPE-BSAL, however, was relatively low compared to MCM-41, which might be because of the filling of the MCM-41mesoporous honeycomb structure(Abbas *et al*., 2020b). The high angle XRD pattern, Fig. 3, showed a broad peak at 22°, which was observed due to the amorphous structures of the MCM-41, MCM-41@NTPE, and MCM-41@NTPE-BSAL (Mohsin & Mihsen, 2020).

3.2.3. N2 Adsorption-Desorption Analysis

The pore volume and surface area of (MCM-41@NTPE and MCM-41@NTPE-BSAL) decreased significantly compared to MCM-41, which has a pore volume of 126.12 $cm^3 \cdot g^{-1}$ and surface area of 548.92 $m^2 \cdot g^{-1}$. This means that the hexagonal pores in the surface are being blocked by large ligand molecules N-[3-(Trimethoxysilyl)propyl]ethylenediamine, causing the surface to be over crowded with the ligand network on the surface and thus blocking the pores.However, a hysteresis loop was detected for both MCM-41@NTPE and MCM-41@NTPE-BSAL within the range from 0.4 < P/Po < 1, associated with capillary condensation as per the

IUPAC classification. All samples exhibited type III isotherms with H3 hysteresis loops, characteristic of mesoporous solids with a pore width ranging from 4-15 nm (Adam & Iqbal, 2010; Attol *et al*., 2023). Figure 5 shows the pore size distributions of MCM-41@NTPE and MCM-41@NTPE-BSAL. According to the BET plot (Figures 4 and 5), the samples' porosity changed, but they still had a narrow pore width distribution, which is typical for MCM-41 derivative materials (Muniandy *et al*., 2019).

This means that large ligand molecules, namely N, are blocking the hexagonal pores in the surface-[3-(trimethoxysilyl)propyl]ethylenediamine,

causing the surface to become 'overcrowded' with the ligand network, thus blocking the pores (Adam *et al*., 2012).

3.2.4. Analysis of SEM and EDX

It is clear from these images shown in Figure 6 that the particles are smooth with a spherical agglomeration. The average diameter ranges between 20-100 nm, corresponding to mesoporous and macroporous materials (Barrett *et al*., 1951; Lee *et al*., 1995). According to EDX analysis, the presence of silicon, oxygen, and nitrogen was demonstrated in the solid ligand (MCM-41@NTPE), as shown in Figure 7. From this, it can be further concluded that the MCM-41 was incorporated into the *N*-[3-(trimethoxysilyl)propyl]ethylenediamine. The analysis of this spectrum(EDX analysis) revealed that the compounds contained carbon, nitrogen, and bromine, in addition to oxygen and silicon in the complex, from which it can be further concluded that the 5-bromosalicylaldehyde was incorporated onto the MCM-41@NTPE.

3.2.5. TEM Microscopy

From Figure 8, the TEM images of MCM-41@NTPE and MCM-41@NTPE-BSAL indicate hexagonal honeycomb structures (Abbas *et al*., 2020b; Appaturi *et al*., 2012; Kamari & Ghorbani, 2021). The honeycomb structure of the MCM-41@NTPE and MCM-41@NTPE-BSAL was not preserved after the functionalization of MCM-41 with *N*-[3-(trimethoxysilyl)propyl] ethylenediamine and then with 5-bromosaliyaldehyde. This is because the immobilization of big organic compounds on the MCM-41 caused the surface to become too crowded with the ligand network, blocking the pores. Also, all species exhibited ordered porous structures, which is consistent with previous work on MCM-41 (Appaturi & Adam, 2013). The TEM images showed the multifarious layers of the accumulated ordered pores in the structures of MCM-41@NTPE and MCM-41@NTPE-BSAL.

3.2.6. AFM Analysis

It was found that the two-dimensional images of the MCM-41@NTPE and MCM-41@NTPE-BSAL topographies were not clear (Figure 9), while three-dimensional images showed a high and a low topography responsible for the surface roughness of the silica. Table 1 shows the parameters obtained from AFM for the prepared MCM-41@NTPE and MCM-41@NTPE-BSAL surfaces. It is clear from this table that the roughness factor is high for MCM-41@NTPE but decreased upon functionalization from 1.161 nm to 429.4 pm. This change may be attributed to the successful modification of the surface of the ligand between MCM-41 and MCM-41@NTPE; the roughness factor of MCM-41@NTPE-BSAL was low, so it can be inferred that its topography is smooth, which is clear in all its electron microscopy (SEM, TEM, and AFM).

3.2.7. Thermal Analysis

The TGA results (Figure 10) showed three mass production stages at approximately 15-900 °C. The initial step(10%) involved the elimination of physically/chemically adsorbed water on the surface of the silica, whilst the second(10%) was assigned to the decomposition of organic moiety for MCM-41@NTPE and MCM-41@NTPE-BSAL. The third step(33%) and (38%)respectively for MCM-41@NTPE and MCM-41@NTPE-BSAL involved the breakdown of Si-OH groups in the silica structure and their transformation into Si-O-Si siloxane groups (Rout *et al*., 2020; Vaysipour *et al*., 2020).

3.2.8. Adsorption studies

3.2.8.1 Effect of Exposure Time

It was demonstrated that there was a nonlinear increase in the uptake of metal ions as a function of the exposure time due to the diffusion factors (Figure 11). This increase can be characterized as a fast initial uptake followed by a period of constant uptake due to blocking the pores, thus inhibiting further contact between metal ions and unreacted amine groups. This perspective aligns with the conclusions offered by other researchers (Yang *et al*., 1997)

3.2.8.2 Effect of pH

The pH influences the adsorbent and the adsorbent surface, where the hydroxide and hydrogen ions compete for the adsorbing surface. Thus, a change in the acidity of the solution can

affect the adsorption process negatively or positively (Ouyang *et al*., 2019). It is usually assumed that when the pH is lower, more hydrogen will be concentrated on the surfaces of the MCM-41@NTPE and MCM-41@NTPE-BSAL, leading to strong competition between the released proton and metal ions for the active site on the surface, causing more free metal ions to remain in solution (Witek-Krowiak *et al*., 2011). After the highest value of uptake, there is no change due to the production of metal oxide (El-Nahhal *et al*., 2000). The uptake of the divalent metal ions increases in the order Cu(II) **>** Co(II). The order of metal uptake capacities agrees with the stability constants established by Irving William and the acid-base concept developed by Pearson (El-Ashgar *et al*., 2018)

3.2.8.3 Effect of Concentration of Co(II) and Cu(II) Ions

Figures 14 and 15 demonstrated that the uptake increased with increasing concentrations of Co(II) and Cu(II) ions at various times (Yang *et al*., 1997). The uptake increased with increasing concentration of each metal ion; this is possible because each ion forms a 1:1 complex with the ligand at high concentration, but when the concentration of ion is low, there is only a minimal amount of uptake due to the formation of a 1:2 complex (Al-Abbasy, 2019). Increasing metal ion concentration leads to better uptake efficiency because higher concentrations of metal occupy a larger number of binding sites, which results in increased uptake (Georgin *et al*., 2016).

3.2.8.4 Effect of mass of the MCM-41@NTPE and MCM-41@NTPE-BSAL.

Maximum uptake of Co(II) and Cu(II) ions was observed for 0.2 g of both MCM-41@NTPE and MCM-41@NTPE-BSAL. This finding (Figures 16 and 17) demonstrated a progressive increase in the uptake of metal ions as the quantity of adsorbent was increased (Al-Abbasy, 2019). However, a subsequent increase in adsorbent will not affect the uptake of Co(II) ions from the solution. This may be due to the blocking of donor sites of the solid ligand by the same ligand(Al-Abbasy, 2019). The results also showed that MCM-41@NTPE-BSAL is more efficient concerning the uptake of Co(II) and Cu(II) ions in solution than APMCM uptake when the adsorbent dosage was increased.

The metal ion uptake capacity (Co^{2+} and Cu^{2+}) as mmol M^{2+}/g ligand, was determined by shaking the functionalized ligand system with metal ion solutions.The results in mmol M^{2+}/g ligand are given in Table 2 comparison of various adsorbents for ions adsorption .

4. CONCLUSIONS

In this research, two types of mesoporous silica (MCM-41@NTPE and MCM-41@NTPE-BSAL) were prepared using silica extracted from rice husk by functionalization of MCM-41. These species were characterized via FT-IR, XRD, N_2 adsorption-desorption, FESEM, EDX, TEM, and TGA/DTA analysis.

The findings indicated that MCM-41@NTPE and MCM-41@NTPE-BSAL had been synthesized with highly ordered hexagonal arrangements. BET analysis was conducted to determine specific surface area, average pore diameter, and total pore volume. XRD diffraction analysis revealed that MCM-41@NTPE and MCM-41@NTPE-BSAL displayed certain amorphous natures. Thermogravimetric analysis suggested that MCM-41@NTPE and MCM-41@NTPE-BSAL have the potential to remain stable, although they decompose within the temperature range of 15-900 °C. The solid materials demonstrated a high efficacy in uptake and extracting copper and cobalt ions from an aqueous solution. Different applications, such as acting as adsorbents for heavy metals, were found as potential applications for MCM-41@NTPE and MCM-41@NTPE-BSAL, where it was also found that the uptake of ions by MCM-41@NTPE-BSAL was better than for MCM-41@NTPE.

5. DECLARATIONS

5.1. Study Limitations

No limitations were known at the time of the study.

5.2. Acknowledgements

The authors of the current research paper would like to thank Kerbala University, College of Science, Department of Chemistry for financial support.

5.3. Funding source

The authors funded this research.

5.4. Competing Interests

The authors declare that they have no conflicts of interest.

6. REFERENCES:

1. Abbas, S. H., Adam, F., & Muniandy, L. (2020a). Green synthesis of MCM-41 from rice husk and its functionalization with nickel(II) salen complex for the rapid catalytic oxidation of benzyl alcohol. *Microporous and Mesoporous Materials*, *305*. https://doi.org/10.1016/j.micromeso.2020.110192
2. Adam, F., Andas, J., & Rahman, I. A. (2010a). A study on the oxidation of phenol by heterogeneous iron silica catalyst. In *Chemical Engineering Journal* (Vol. 165, Issue2,pp.658–667). https://doi.org/10.1016/j.cej.2010.09.054
3. Adam, F., & Batagarawa, M. S. (2013). Tetramethylguanidine–silica nanoparticles as an efficient and reusable catalyst for the synthesis of cyclic propylene carbonate from carbon dioxide and propylene oxide. *Applied Catalysis A: General*, *454*, 164–171. https://doi.org/10.1016/j.apcata.2012.12.009
4. Adam, F., Hello, K. M., & Chai, S.-J. (2012). The heterogenization of l-phenylalanine–Ru (III) complex and its application as catalyst in esterification of ethyl alcohol with acetic acid. *Chemical Engineering Research and Design*, *90*(5), 633–642. https://doi.org/10.1016/j.cherd.2011.09.009
5. Adam, F., & Iqbal, A. (2010). The oxidation of styrene by chromium–silica heterogeneous catalyst prepared from rice husk. *Chemical Engineering Journal*, *160*(2), 742–750. https://doi.org/10.1016/j.cej.2010.04.003
6. Al-Abbasy, D. H. A. (2019). Synthesis and Characterization of Organosilicon Ligands and Used It in Removal of Some Divalent Metal Ions from Their Aqueous Solutions. *University of Kerbala*.
7. Ali, H. H., Hussein, K. A., & Mihsen, H. H. (2023). Antimicrobial Applications of Nanosilica Derived from Rice Grain Husks. *Silicon*, *0123456789*. https://doi.org/10.1007/s12633-023-02467-7.
8. Appaturi, J. N., & Adam, F. (2013). A facile and efficient synthesis of styrene carbonate via cycloaddition of CO2 to styrene oxide over ordered mesoporous MCM-41-Imi/Br catalyst. *Applied Catalysis B: Environmental*, *136–137*, 150–159. https://doi.org/10.1016/j.apcatb.2013.01.049
9. Appaturi, J. N., Adam, F., & Khanam, Z. (2012). A comparative study of the regioselective ring opening of styrene oxide with aniline over several types of mesoporous silica materials. *Microporous and Mesoporous Materials*, *156*, 16–21. https://doi.org/10.1016/j.micromeso.2012.01.023
10. Attol, D. H., Mihsen, H. H., Jaber, S. A., Alwazni, W. S., & Eesa, M. T. (2023). Synthesis of Organic Functionalized Silica from Rice Husk as an Antibacterial Agents. *Silicon*, *15*(5),2349–2357. https://doi.org/10.1007/s12633-022-02194-5
11. Barczak, M., Dobrowolski, R., Borowski, P., & Giannakoudakis, D. A. (2020). Pyridine-, thiol- and amine-functionalized mesoporous silicas for adsorptive removal of pharmaceuticals. *Microporous and Mesoporous Materials*, *299*, 110132. https://doi.org/10.1016/j.micromeso.2020.110132
12. Barrett, E. P., Joyner, L. G., & Halenda, P. P. (1951). The determination of pore volume and area distributions in porous substances. I. Computations from nitrogen isotherms. *Journal of the American Chemical Society*, *73*(1),373–380. https://doi.org/10.1021/ja01145a126

13. Bernardoni, F., & Fadeev, A. Y. (2011). Adsorption and wetting characterization of hydrophobic SBA-15 silicas. *Journal of Colloid and Interface Science*, *356*(2), 690–698. https://doi.org/10.1016/j.jcis.2011.01.033

14. Carmona, V. B., Oliveira, R. M., Silva, W. T. L., Mattoso, L. H. C., & Marconcini, J. M. (2013). Nanosilica from rice husk: extraction and characterization. *Industrial Crops and Products*,*43*,291–296. https://doi.org/10.1016/j.indcrop.2012.06.050

15. Chong, A. S. M., Zhao, X. S., Kustedjo, A. T., & Qiao, S. Z. (2004). Functionalization of large-pore mesoporous silicas with organosilanes by direct synthesis. *Microporous and Mesoporous Materials*,*72*(1–3),33–42. https://doi.org/10.1016/j.micromeso.2004.04.015

16. Costa, J. A. S., Vedovello, P., & Paranhos, C. M. (2020). Use of Ionic Liquid as Template for Hydrothermal Synthesis of the MCM-41 Mesoporous Material. *Silicon*, *12*(2), 289–294. https://doi.org/10.1007/s12633-019-00121-9

17. Dragoi, B., Dumitriu, E., Guimon, C., & Auroux, A. (2009). Acidic and adsorptive properties of SBA-15 modified by aluminum incorporation. *Microporous and Mesoporous Materials*, *121*(1–3), 7–17. https://doi.org/10.1016/j.micromeso.2008.12.023

18. El-Ashgar, N. M., El-Nahhal, I. M., Ahmed, M. A., Abu Shaweesh, A. A., & Chehimi, M. M. (2018). Synthesis, characterization, and metal uptake of multiple functionalized immobilized-polysiloxane diamine-thiol chelating ligand derivatives. *Journal of the Iranian Chemical Society*, *15*(10), 2325–2338. https://doi.org/10.1007/s13738-018-1421-0

19. El-Ashgar, N. M., El-Nahhal, I. M., Chehimi, M. M., Babonneau, F., & Livage, J. (2007). A new route synthesis of immobilized-polysiloxane iminodiacetic acid ligand system, its characterization and applications. *Materials Letters*, *61*(23–24), 4553–4558. https://doi.org/10.1016/j.matlet.2007.02.050

20. El-Kurd, H. M., El-Nahhal, I. M., & El-Ashgar, N. M. (2005). Synthesis of new polysiloxane-immobilized ligand system di (amidomethyl) aminetetraacetic acid. *Phosphorus, Sulfur, and Silicon*, *180*(7), 1657–1671. https://doi.org/10.1080/104265090885084

21. El-Nahhal, I. M., El-Ashgar, N. M., Chehimi, M. M., Bargiela, P., Maquet, J., Babonneau, F., & Livage, J. (2003). Metal uptake by porous iminobis (N-2-aminoethylacetamide)-modified polysiloxane ligand system. Microporous and Mesoporous Materials, 65(2–3),299–310. https://doi.org/10.1016/S1387-1811(03)0 0 5 03-1

22. El-Nahhal, I. M., El-Shetary, B. A., Mustafa, A. E.-K. B., El-Ashgar, N. M., Livage, J., Chehimi, M. M., & Roberts, A. (2003). Structural characterization of immobilized-polysiloxane iminobis (N-diethylenediamineacetamide) ligand system. *Solid State Sciences*, *5*(10), 1395–1406. https://doi.org/10.1016/S1293-2558(03)00195-X

23. El-Nahhal, I. M., Zaggout, F. R., & El-Ashgar, N. M. (2000). Uptake of divalent metal ions (Cu2+, Zn2+ and Cd2+) by polysiloxane immobilized monoamine ligand system. In *Analytical Letters* (Vol. 33, Issue 10, pp. 2031–2053). https://doi.org/10.1080/00032710008543173

24. Georgin, J., Dotto, G. L., Mazutti, M. A., & Foletto, E. L. (2016). Preparation of activated carbon from peanut shell by conventional pyrolysis and microwave irradiation-pyrolysis to remove organic dyes from aqueous solutions. *Journal of Environmental Chemical Engineering*, *4*(1), 266–275. https://doi.org/10.1016/j.jece.2015.11.018

25. Kamari, S., & Ghorbani, F. (2021). Extraction of highly pure silica from rice husk as an agricultural by-product and its application in the production of magnetic mesoporous silica MCM–41. *Biomass Conversion and Biorefinery*, *11*, 3001–3009. https://doi.org/10.1007/s13399-020-00637-w

26. Kim, S., Ida, J., Guliants, V. V, & Lin, Y. S. (2005). Tailoring pore properties of MCM-48 silica for selective adsorption of CO2.

The Journal of Physical Chemistry B, *109*(13), 6287–6293. https://doi.org/10.1021/jp045634x

27. Lee, C. K., Chiang, A. S. T., & Tsay, C. S. (1995). The Characterization of Porous Solids from Gas Adsorption Measurements. *Key Engineering Materials*, *115*, 21–44. https://doi.org/10.4028/www.scientific.net/KEM.115.21
28. Li, J., Qi, T., Wang, L., Liu, C., & Zhang, Y. (2007). Synthesis and characterization of imidazole-functionalized SBA-15 as an adsorbent of hexavalent chromium. *Materials Letters*, *61*(14–15), 3197–3200. https://doi.org/10.1016/j.matlet.2006.11.079
29. Luan, Z., Fournier, J. A., Wooten, J. B., & Miser, D. E. (2005). Preparation and characterization of (3-aminopropyl) triethoxysilane-modified mesoporous SBA-15 silica molecular sieves. *Microporous and Mesoporous Materials*, *83*(1–3), 150–158. https://doi.org/10.1016/j.micromeso.2005.04.006
30. Martínez-Carmona, M., Ho, Q. P., Morand, J., García, A., Ortega, E., Erthal, L. C. S., Ruiz-Hernandez, E., Santana, M. D., Ruiz, J., Vallet-Regí, M., & Gun'ko, Y. K. (2020). Amino-Functionalized Mesoporous Silica Nanoparticle-Encapsulated Octahedral Organoruthenium Complex as an Efficient Platform for Combatting Cancer. *Inorganic Chemistry*, *59*(14), 10275–10284. https://doi.org/10.1021/acs.inorgchem.0c01436
31. Mirji, S. A., Halligudi, S. B., Sawant, D. P., Jacob, N. E., Patil, K. R., Gaikwad, A. B., & Pradhan, S. D. (2006). Adsorption of octadecyltrichlorosilane on mesoporous SBA-15. *Applied Surface Science*, *252*(12), 4097–4103. https://doi.org/10.1016/j.apsusc.2005.06.009
32. Mohsin, A. D., & Mihsen, H. H. (2020). Uptake of metal ions (Co (II) and Ni (II)) by silica-salicylaldehyde derived from rice husks. *Journal of Inorganic and Organometallic Polymers and Materials*, *30*, 2172–2181. https://doi.org/10.1007/s10904-019-01379-7
33. Muniandy, L., Adam, F., Rahman, N. R. A., & Ng, E. P. (2019). Highly selective synthesis of cyclic carbonates via solvent free cycloaddition of CO 2 and epoxides using ionic liquid grafted on rice husk derived MCM-41. *Inorganic Chemistry Communications*, *104*, 1–7. https://doi.org/10.1016/j.inoche.2019.03.012
34. Mureseanu, M., Reiss, A., Stefanescu, I., David, E., Parvulescu, V., Renard, G., & Hulea, V. (2008). Modified SBA-15 mesoporous silica for heavy metal ions remediation. *Chemosphere*, *73*(9), 1499–1504. https://doi.org/10.1016/j.chemosphere.2008.07.039
35. Nie, W., Luo, Y., Yang, Q., Feng, G., Yao, Q., & Lu, Z.-H. (2020). An amine-functionalized mesoporous silica-supported PdIr catalyst: boosting room-temperature hydrogen generation from formic acid. *Inorganic Chemistry Frontiers*, *7*(3), 709–717. https://doi.org/10.1039/C9QI01375J
36. Ouyang, D., Zhuo, Y., Hu, L., Zeng, Q., Hu, Y., & He, Z. (2019). Research on the Adsorption Behavior of Heavy Metal Ions by Porous Material Prepared with Silicate Tailings. *Minerals*, *9*(5), 291. https://doi.org/10.3390/min9050291
37. Pérez-Quintanilla, D., Del Hierro, I., Fajardo, M., & Sierra, I. (2006). Mesoporous silica functionalized with 2-mercaptopyridine: Synthesis, characterization and employment for Hg (II) adsorption. *Microporous and Mesoporous Materials*, *89*(1–3), 58–68. https://doi.org/10.1016/j.micromeso.2005.10.012
38. Pervaiz, M., Ahmad, I., Yousaf, M., Kirn, S., Munawar, A., Saeed, Z., Adnan, A., Gulzar, T., Kamal, T., Ahmad, A., & Rashid, A. (2019). Synthesis, spectral and antimicrobial studies of amino acid derivative Schiff base metal (Co, Mn, Cu, and Cd) complexes. *Spectrochimica Acta Part A: Molecular and Biomolecular Spectroscopy*, *206*, 642–649. https://doi.org/10.1016/j.micromeso.2020.110192
39. Rout, L., Mohan, A., Thomas, A. M., & Ha, C.-S. (2020). Rational design of thermoresponsive functionalized MCM-41

and their decoration with bimetallic Ag–Pd nanoparticles for catalytic application. *Microporous and Mesoporous Materials*, *291*, 109711. https://doi.org/10.1016/j.micromeso.2019.109711

40. Sutra, P., & Brunel, D. (1996). Preparation of MCM-41 type silica-bound manganese(III) Schiff-base complexes. *Chemical Communications*,*21*,2485. https://doi.org/10.1039/CC9960002485
41. Vaysipour, S., Rafiee, Z., & Nasr-Esfahani, M. (2020). Synthesis and characterization of copper (II)-poly (acrylic acid)/M-MCM-41 nanocomposite as a novel mesoporous solid acid catalyst for the one-pot synthesis of polyhydroquinoline derivatives. *Polyhedron*, *176*,114294. https://doi.org/10.1016/j.poly.2019.114294
42. Verma, P., Kuwahara, Y., Mori, K., Raja, R., & Yamashita, H. (2020). Functionalized mesoporous SBA-15 silica: recent trends and catalytic applications. *Nanoscale*, *12*(21), 11333–11363. https://doi.org/10.1039/D0NR00732C
43. Wang, X., Du, X., Li, C., & Cao, X. (2008). Direct synthesis and characterization of phenyl-functionalized SBA-15. *Applied Surface Science*, *254*(13), 3753–3757. https://doi.org/10.1016/j.apsusc.2007.11.031
44. Witek-Krowiak, A., Szafran, R. G., & Modelski, S. (2011). Biosorption of heavy metals from aqueous solutions onto peanut shell as a low-cost biosorbent. *Desalination*, *265*(1–3), 126–134.
45. Yang, J. J., El-Nahhal, I. M., Chuang, I.-S., & Maciel, G. E. (1997). Synthesis and solid-state NMR structural characterization of polysiloxane-immobilized amine ligands and their metal complexes. *Journal of Non-Crystalline Solids*, *209*(1–2), 19–39. https://doi.org/10.1016/S0022-3093(96)00534-0
46. Yu, H., & Zhai, Q.-Z. (2009). Mesoporous SBA-15 molecular sieve as a carrier for controlled release of nimodipine. *Microporous and Mesoporous Materials*, *123*(1–3), 298–305. https://doi.org/10.1016/j.micromeso.2009.04.013

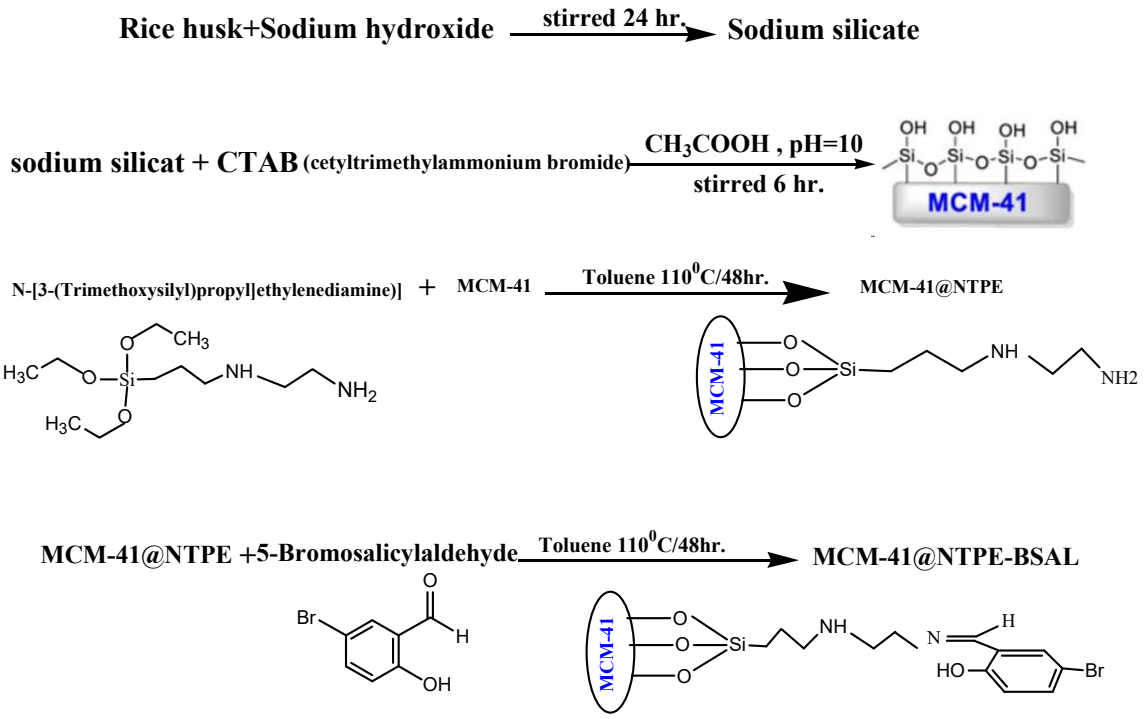

Scheme 1. *The synthesis of MCM-41@NTPE and MCM-41@NTPE-BSAL*

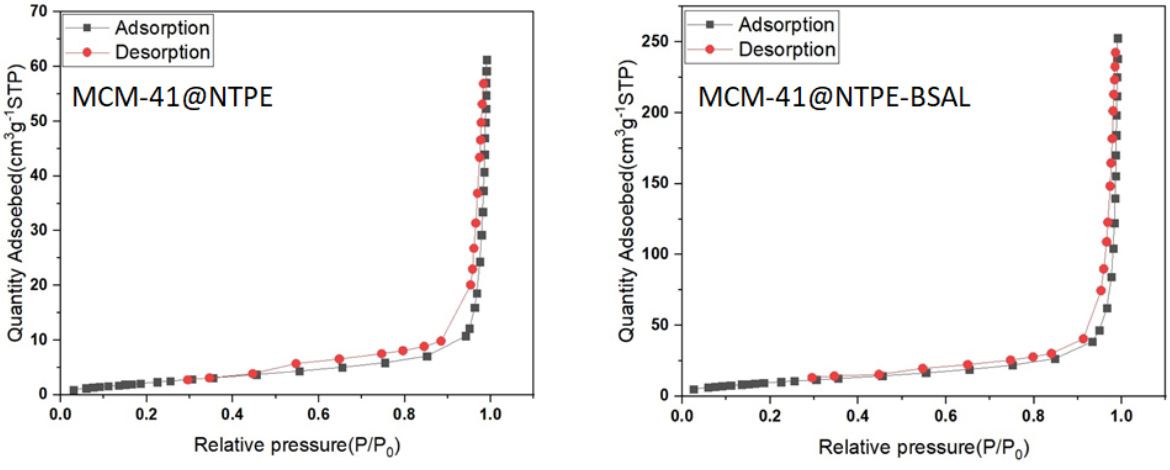

Figure 4: N_2 adsorption–desorption isotherms of MCM-41@NTPEand MCM-41@NTPE-BSAL

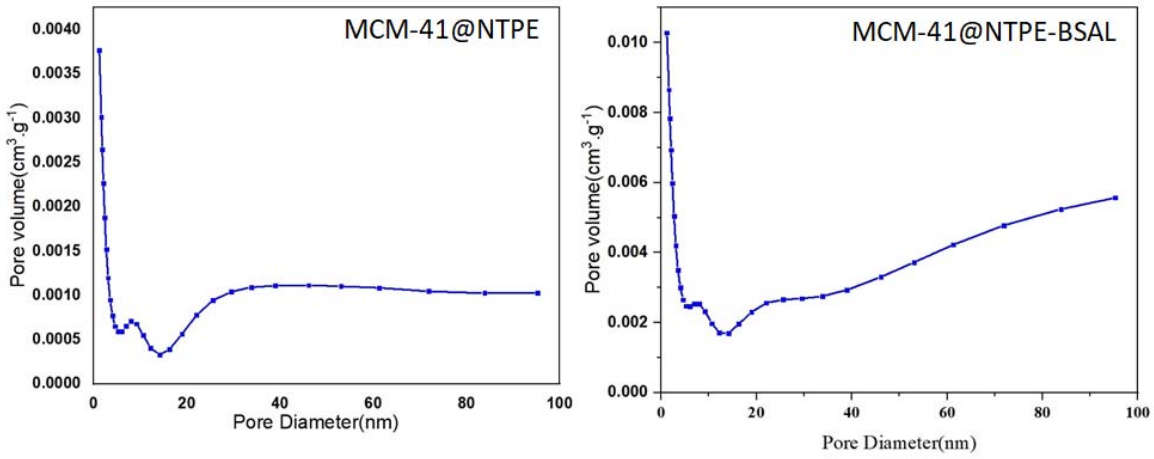

Figure 5: N_2 adsorption–desorption isotherms of MCM-41@NTPEand MCM-41@NTPE-BSAL

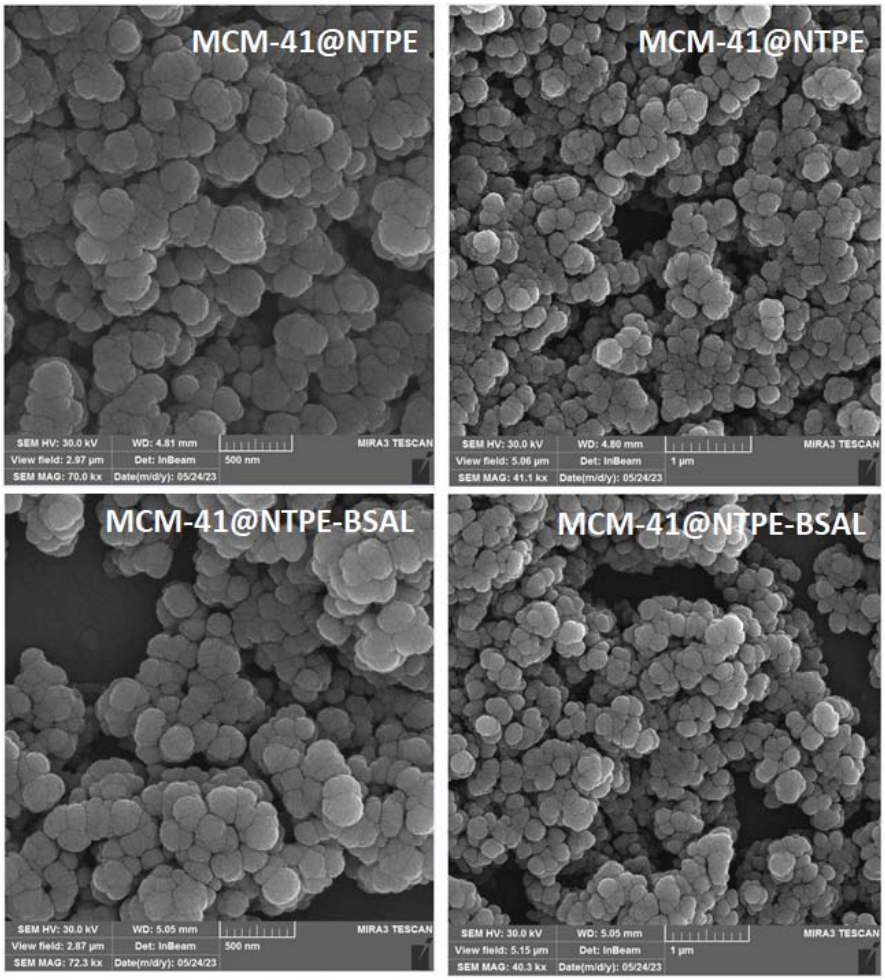

Figure 6: SEM analysis of MCM-41@NTPE and MCM-41@NTPE-BSAL at scales of 500 nm and 1000 nm.

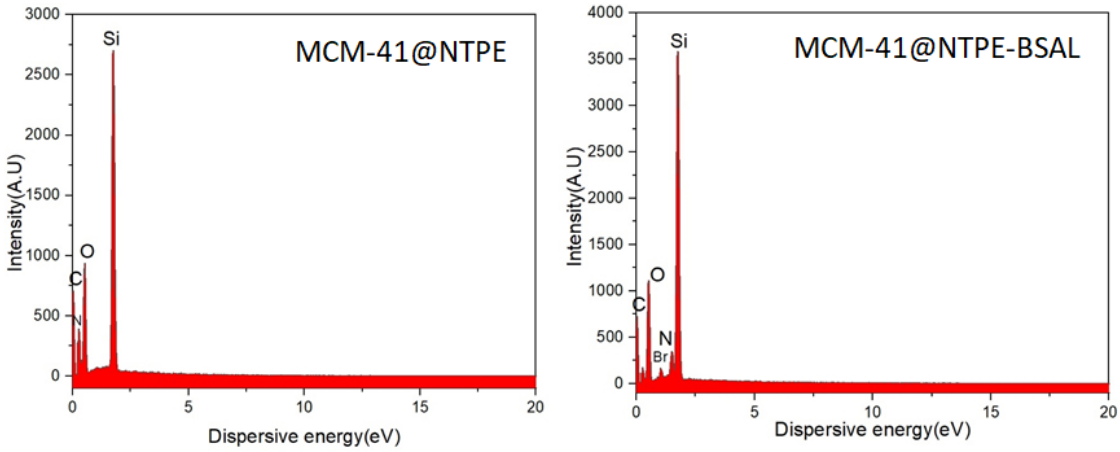

Figure 7: EDX analysis of MCM-41@NTPE and MCM-41@NTPE-BSAL.

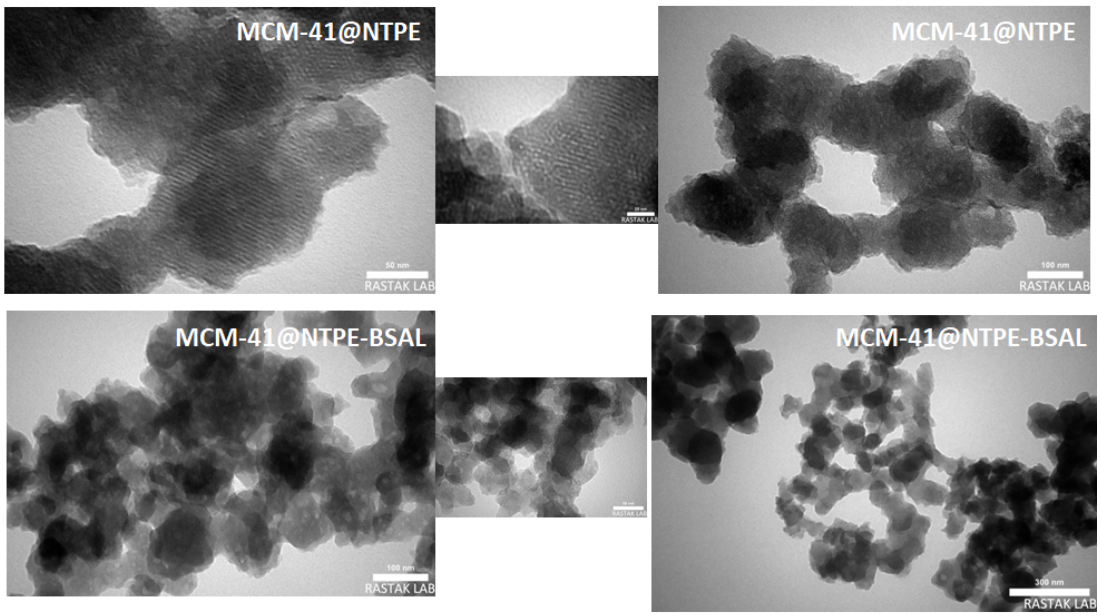

Figure 8: TEM images of MCM-41@NTPE and MCM-41@NTPE-BSAL at different scales.

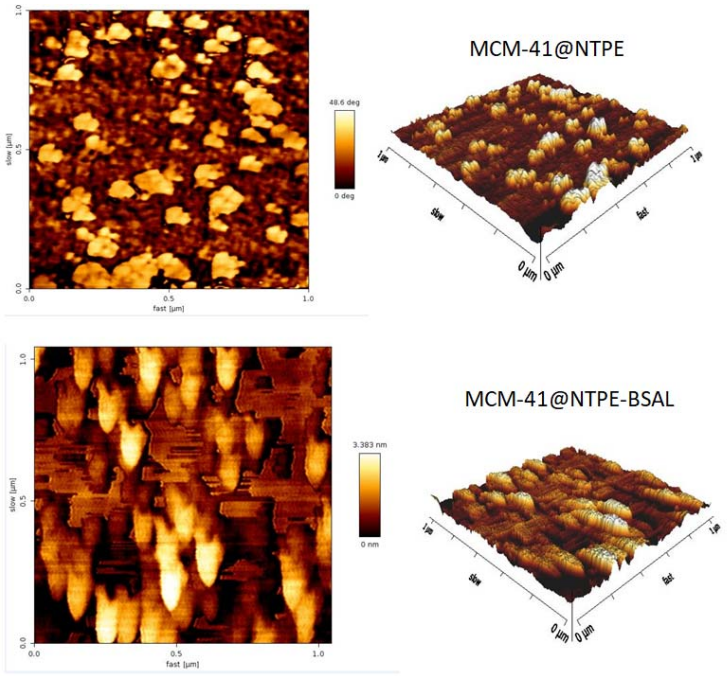

Figure 9: AFM 2D (on the left) and 3D (on the right) micrographs of MCM-41@NTPE and MCM-41@NTPE-BSAL.

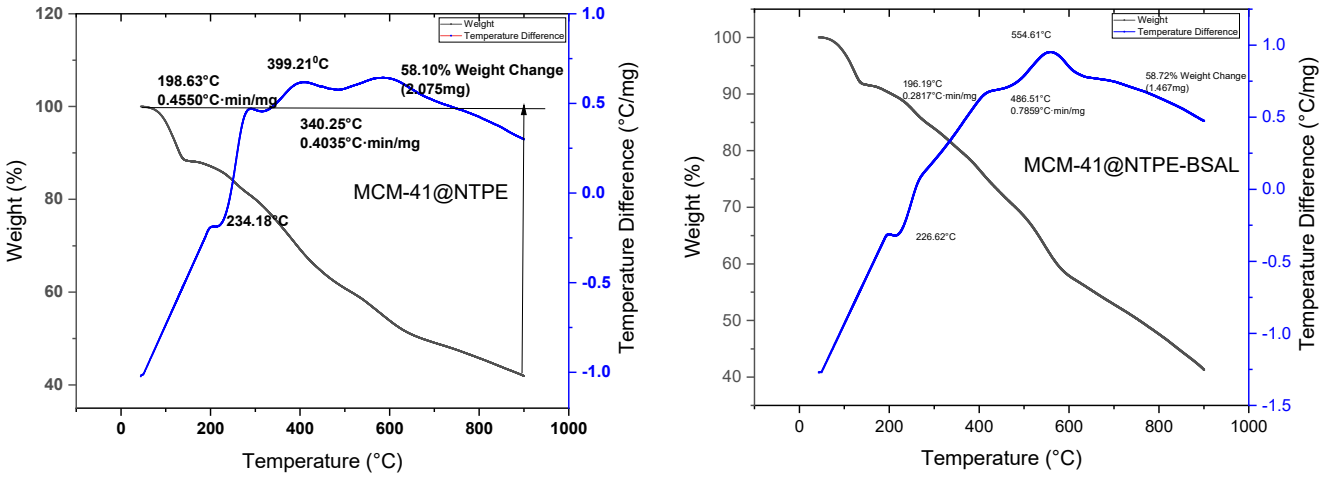

Figure 10: TGA-DTA plots of MCM-41@NTPE and MCM-41@NTPE-BSAL.

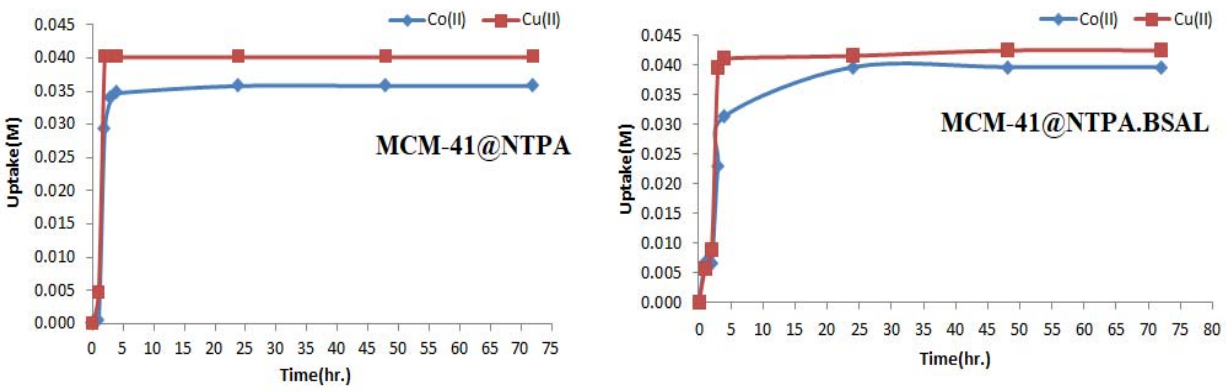

Figure 11: The Co(II) and Cu(II) ions uptake by MCM-41@NTPE and MCM-41@NTPE-BSAL ligand systems versus time.

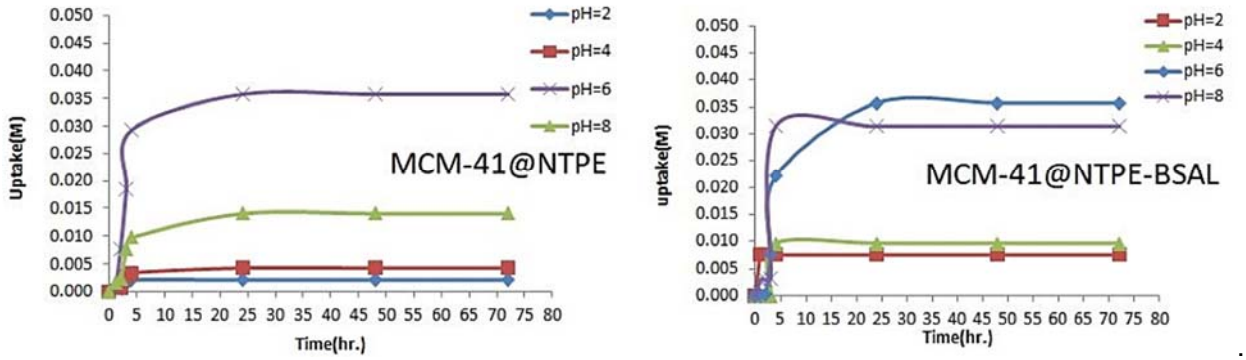

Figure 12: The Co(II) ions uptake by MCM-41@NTPE and MCM-41@NTPE-BSAL at various pHs.

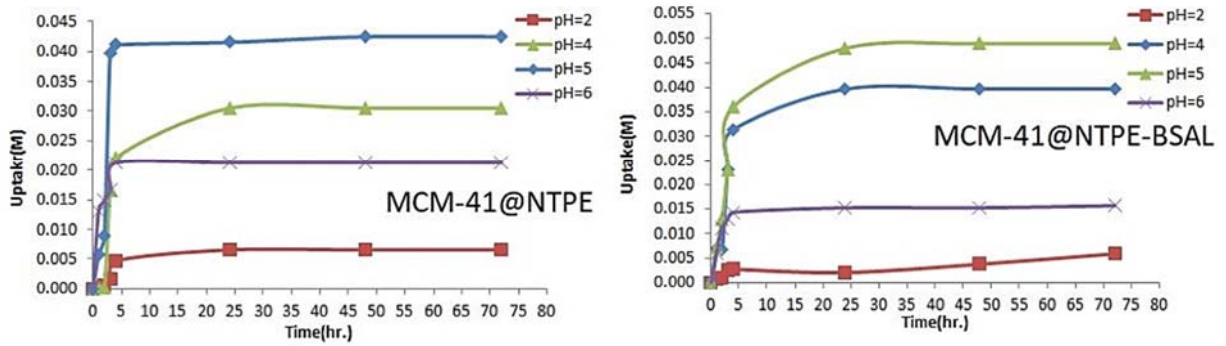

Figure 13: Cu(II) ions uptake by MCM-41@NTPE and MCM-41@NTPE-BSAL at various pHs.

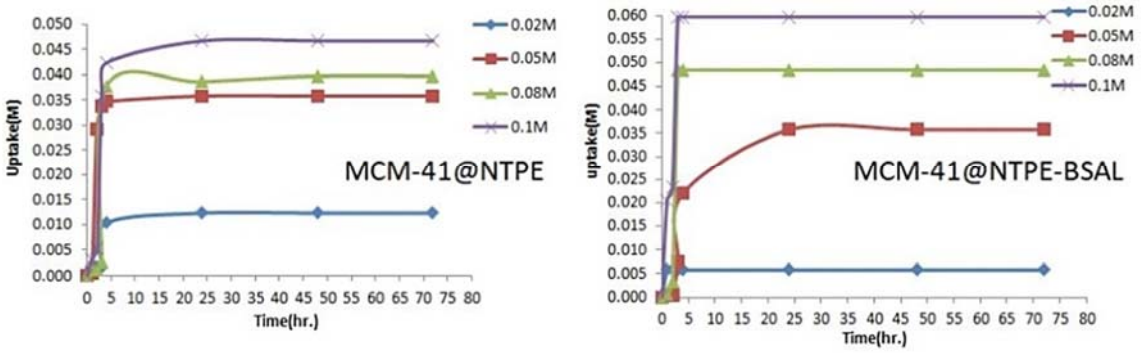

Figure 14: The uptake of Co(II) ions by MCM-41@NTPE and MCM-41@NTPE-BSAL at various initial concentrations

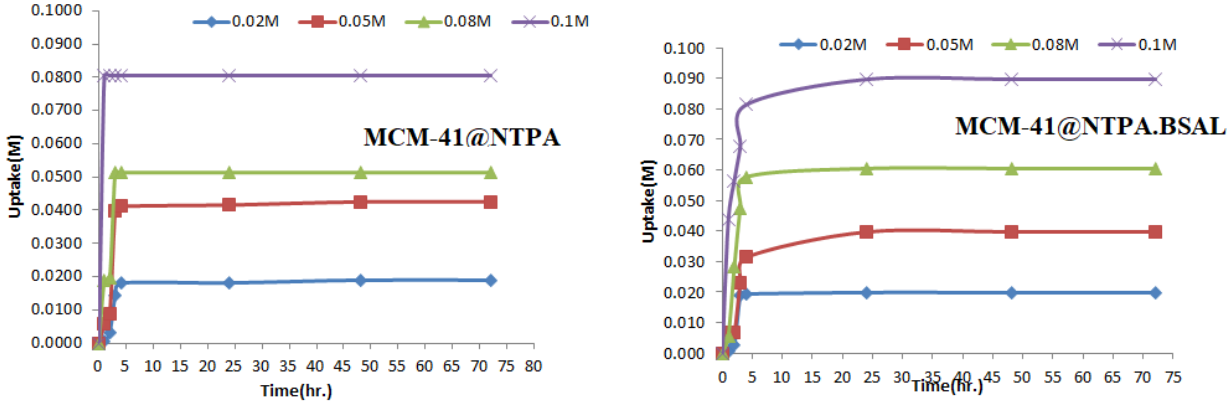

Figure 15: Cu(II) ions uptake by MCM-41@NTPE and MCM-41@NTPE-BSAL at various initial concentrations.

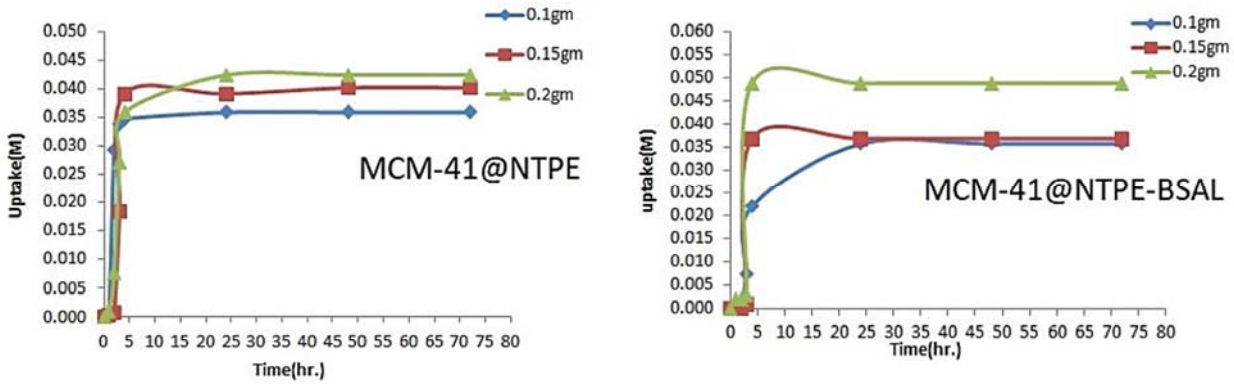

Figure 16: The uptake of Co(II) ions for various masses of MCM-41@NTPE and MCM-41@NTPE-BSAL.

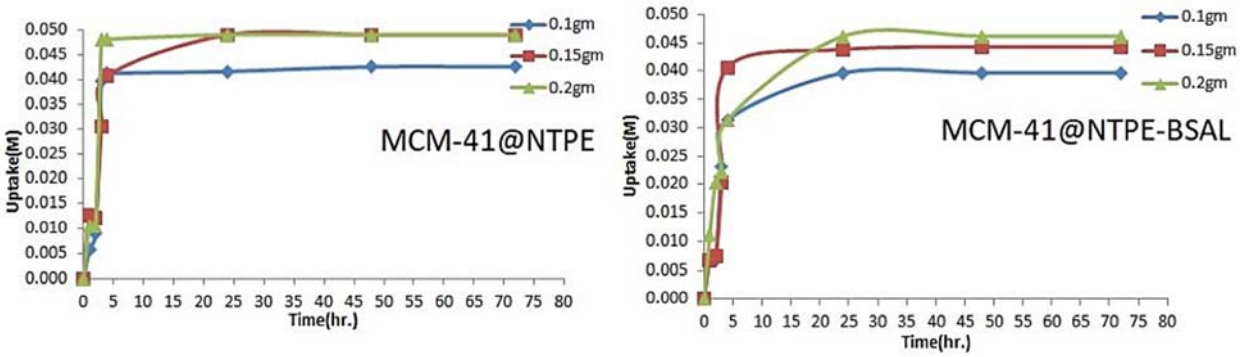

Figure 17: The uptake of Cu(II) ions for various masses of MCM-41@NTPE and MCM-41@NTPE-BSAL.

Table 1. *AFM parameters for MCM-41@NTPE and MCM-41@NTPE-BSAL.*

Sample	Average roughness(Ra)	Root square roughness (Rrms)	Average height (SZ)
MCM-41@NTPE	1.161 nm	1.585 nm	12.09 nm
MCM-41@NTPE-BSAL	429.4 pm	760.8 pm	9.201 nm

Table 2. *Comparison of various adsorbents for ions adsorption.*

	Metals ions		
Maximum uptake (mmol M^{2+}/g ligand)	Cu(II)	Co(II)	Ref.
	2.31	1.73	(El-Ashgar *et al*., 2007)
	2.4	2	(El-Kurd *et al*., 2005)
	1.6	0.9	(El-Nahhal, El-Ashgar, *et al*., 2003)
	1.65	1.52	(El-Nahhal, El-Shetary, *et al*., 2003)
	21	17.5	Present work (MCM-41@NTPE)
	23	18	Present work (MCM-41@NTPE-BSAL)